

Low-temperature dynamics of kinks on Ising interfaces

Alain Karma and Alexander E. Lobkovsky

Department of Physics, Northeastern University, Boston, Massachusetts 02139, USA

(Received 28 July 2004; published 15 March 2005)

The anisotropic motion of an interface driven by its intrinsic curvature or by an external field is investigated in the context of the kinetic Ising model in both two and three dimensions. We derive in two dimensions (2D) a continuum evolution equation for the density of kinks by a time-dependent and nonlocal mapping to the asymmetric exclusion process. Whereas kinks execute random walks biased by the external field and pile up vertically on the physical 2D lattice, they execute hard-core biased random walks on a transformed 1D lattice. Their density obeys a nonlinear diffusion equation which can be transformed into the standard expression for the interface velocity, $v = M[(\gamma + \gamma'')\kappa + H]$, where M , $\gamma + \gamma''$, and κ are the interface mobility, stiffness, and curvature, respectively. In 3D, we obtain the velocity of a curved interface near the $\langle 100 \rangle$ orientation from an analysis of the self-similar evolution of 2D shrinking terraces. We show that this velocity is consistent with the one predicted from the 3D tensorial generalization of the law for anisotropic curvature-driven motion. In this generalization, both the interface stiffness tensor and the curvature tensor are singular at the $\langle 100 \rangle$ orientation. However, their product, which determines the interface velocity, is smooth. In addition, we illustrate how this kink-based kinetic description provides a useful framework for studying more complex situations by modeling the effect of immobile dilute impurities.

DOI: 10.1103/PhysRevE.71.036114

PACS number(s): 05.70.Np, 05.70.Ln, 68.35.Fx, 68.35.Md

I. INTRODUCTION

Many bulk properties of polycrystals are strongly influenced by the underlying microstructure. Much effort goes into predicting the motion of grain boundaries in response to a variety of driving forces. Depending on the nature of the grains, their boundaries migrate in response to applied stresses [1] or magnetic fields [2], internal forces associated with grain boundary curvature [3], concentration gradients [4], etc. Successful models of microstructure evolution must be supplied with the details of the ways in which the grain boundaries respond to the driving forces.

Based on general conclusions of nonequilibrium statistical mechanics, one would expect the interface to have a unique mobility—i.e., a unique response coefficient to disparate driving forces. This conclusion was recently called into question by both experiments in polycrystals [5,6] and simulations of Ising interfaces [7]. These works observed drastically different shapes of shrinking grains. Grains shrinking under the influence of capillarity alone was roughly circular whereas the presence of other driving forces resulted in strongly anisotropic shapes. This observation was most simply interpreted in terms of different interfacial mobilities for different driving forces. A resolution of this apparent paradox in the Ising model [8], which does not require a nonunique mobility, rests with identifying the crucial role of anisotropy in the calculation of the capillary driving force. This driving force is the strongly anisotropic interfacial stiffness [3]—i.e., the sum $\gamma + \gamma''$ of the excess free energy of the interface γ and its second derivative with respect to inclination, rather than γ itself which is much less anisotropic. It turns out that the reduced mobility—i.e., the product of the capillary driving force and the bare mobility—is roughly isotropic, and therefore the grain shape is isotropic as well. Here we shed further light on the microscopic mechanism for cancellation of the anisotropies of the interfacial stiffness and the interfa-

cial mobility in both two and three dimensions (2D and 3D).

The precise microscopic mechanisms responsible for the migration of grain boundaries are complex. However, there is hope that generic features near equilibrium are shared by a large class of models of moving interfaces. It is with this hope in mind we use the kinetic Ising model (KIM), introduced in Ref. [9], as a proxy for studying grain boundaries. The KIM is defined by a collection of spins $s_i = \pm 1$ on a lattice, a total energy which is a function of this collection, and rules for dynamic evolution of the spins at some temperature $\beta = 1/kT$. The energy in the presence of a magnetic field H is

$$E = -J \sum_{\langle ij \rangle} s_i s_j - H \sum_i s_i, \quad (1)$$

where the sum in the first term in Eq. (1) is over pairs of nearest neighbors. Glauber dynamics [9] is one possible scheme for evolving the collection of spins in such a way as to obtain correct distributions in equilibrium. This model is perhaps the simplest representation of the nonequilibrium dynamics of interfaces. It can be used to explore the effects of lattice anisotropy on the motion of domain walls driven by a magnetic field or capillary forces. In addition, domain nucleation and late stages of phase separation can be addressed within the KIM. With simple modifications the KIM can be used to study the phenomenology of interface motion in the presence of mobile or quenched impurities.

Much is known about the equilibrium behavior of Ising interfaces. For example, an exact expression for the interfacial free energy has been derived in 2D on a square lattice [10,11]. Approximate expressions for this free energy and critical amplitudes in 3D have also been derived [12,13]. The nonequilibrium behavior of the KIM is more complicated. Whereas several approximate analytic results exist for the

mobility of a domain wall in 2D [14–16], little progress has been achieved in 3D.

Here we construct a simple and intuitive kinetic description of low-temperature domain walls in the KIM based on the kink degrees of freedom. The density of kinks is shown to obey a nonlinear diffusion equation, which is equivalent to the law of anisotropic interface motion driven by curvature and/or an external field, derived from the interface free energy and mobility. It is important to emphasize that, in our kink description, we obtain the law of interface motion directly in the continuum limit *without* these expressions as input into our calculation. Hence, our kink-based theory can be viewed as a direct microscopic derivation of the law of interface motion in the low-temperature limit of the KIM, free of extraneous assumptions. Moreover, the kink-based description is useful for analyzing more complicated situations. We illustrate this point both by extending the analysis of anisotropic interface motion to 3D and by examining impurity effects in 2D.

Section II of this paper is devoted to the 2D KIM while the following Sec. III extends our results to 3D. In Sec. II A, we review the existing results concerning the KIM in 2D with the focus on the nonequilibrium response of an interface to curvature and magnetic field. In Sec. II B, we rederive the velocity of a curved Ising domain wall driven by capillary forces using kinks as the degrees of freedom responsible for the motion of the interface. This description is accurate at low temperatures when the rate of nucleation of kink-antikink pairs is small. We obtain the shape of a shrinking Ising grain analytically in Sec. II C. In the following Sec. II D we illustrate the usefulness of the kink description by considering the influence of impurities on the grain boundary motion. In Sec. III, we study curvature driven motion in 3D near a high-symmetry singular orientation where the interface can be represented by a collection of terraces composed of kinks. This allows us to use the 2D analytic results to calculate the interface velocity and therefore the mobility tensor near this symmetry direction. Finally, conclusions are given in Sec. IV.

II. TWO-DIMENSIONAL KINETIC ISING MODEL

A. Low-temperature expansion of the interface free energy and mobility

Let us summarize the analytical results obtained so far for the KIM, focusing on the expressions that have been derived for the interface mobility. In 2D, the exact interfacial free energy is known [10,11]. For our purposes it suffices to write down the first two terms in the temperature expansion (enthalpic and entropic respectively). When the spins are arranged on a square (denoted by a \square) lattice of unit lattice spacing, this energy is

$$\gamma_{2D}^{\square}(\phi) = 2J(c+s) + \frac{1}{\beta} [c \ln c + s \ln s - (c+s) \ln(c+s)], \quad (2)$$

where $c = |\cos \phi|$, $s = |\sin \phi|$, and ϕ is the inclination defined as the angle of the interface normal with respect to the $\langle 10 \rangle$ axis of the underlying lattice.

When spins flip according to nonconserved Glauber dynamics [9], the interface moves to minimize the free energy of the system which consists of the bulk and interface contributions. Spohn [14] has derived the sharp interface continuum description of a domain wall in the KIM. It follows from his derivation that the normal velocity of the interface v is the product of the mobility M and a driving force. From the continuum description it also follows that in the absence of magnetic field, the driving force is the product of the mean curvature of the interface κ and the interface stiffness. In 2D, the stiffness is $\gamma + \gamma''$, where γ'' denotes the second derivative of γ with respect to ϕ . Using a Green-Kubo perturbative formalism, Spohn obtained the interface mobility in the limit of small temperature and small driving magnetic field. The same result was obtained earlier by Barma [15] using a mapping of the dynamics of the low-temperature Ising interface to the one-dimensional exclusion process. Rikvold and Kolesik obtained analytical expressions valid for large fields and temperatures [16]. The leading term in the temperature expansion of the mobility diverges like $1/T$:

$$M_{2D}^{\square}(\phi) = \frac{\beta}{2\tau} \frac{|\sin 2\phi|}{|\cos \phi| + |\sin \phi|},$$

$$M_{2D}^{\Delta}(\phi) = \frac{\beta\sqrt{3}}{2\tau} \frac{\sin \phi \left(\cos \phi - \frac{1}{\sqrt{3}} \sin \phi \right)}{\cos \phi + \frac{1}{\sqrt{3}} \sin \phi}, \quad (3)$$

where \square refers to a square lattice and Δ to a triangular lattice. In addition, τ is the intrinsic time scale of the Glauber dynamics which is the inverse frequency of the attempted spin flips. The triangular lattice formula is valid in the $\phi \in [0, \pi/6]$ domain and can be extended to the other angles via an appropriate symmetry transformation.

The above expressions for the interface energy and mobility can be combined to arrive at the continuum (or mean-field) low-temperature equation of motion of the interface driven by curvature κ and magnetic field $H \ll 1/\beta$. The normal velocity of the interface is

$$v_{2D}(\phi) = M_{2D}[\kappa(\gamma_{2D} + \gamma_{2D}'') + H] = M_{2D}^* \kappa + M_{2D} H, \quad (4)$$

where the reduced mobility on the square lattice is (see Appendix A for the triangular lattice result)

$$M_{2D}^*(\phi) \equiv M_{2D}^{\square}(\gamma_{2D} + \gamma_{2D}'') = \frac{1}{\tau(|\cos \phi| + |\sin \phi|)^2}. \quad (5)$$

Note that the reduced mobility is roughly isotropic whereas the bare mobility is strongly anisotropic. In addition, the reduced mobility does not diverge in the $T \rightarrow 0$ limit whereas the bare mobility does. This happens because the contribution of the enthalpic term $2J(c+s)$ to the interfacial stiffness evaluates to zero. Therefore, only the entropic term (which is proportional to T) contributes to the stiffness. Moreover, the contribution due to the entropic term diverges at the high-symmetry orientations whereas the bare mobility vanishes at those orientations in such a way that the product of the two quantities produces a finite nonzero reduced mo-

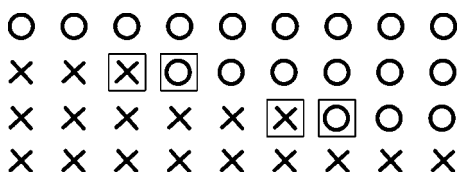


FIG. 1. Schematic description of an interface between up (crosses) and down (circles) spin domains on a square lattice. Only corner (boxed) spins can flip at low temperature. A flip of a corner spin corresponds to moving the kink left or right.

bility. This behavior is responsible for the nearly circular shape of a shrinking grain on a hexagonal lattice in Ref. [7].

B. Direct calculation of M^* via the dynamics of kinks

The basic law of interface motion embodied in Eq. (4) is usually derived using a thermodynamic approach where the interface free energy and mobility are computed separately. This approach, even though general, lacks intuitive appeal. Furthermore, it is not simply extended to more complex situations. It is therefore worthwhile to develop an alternative method for deriving Eq. (5) directly from a microscopic picture without the need to compute the interface free energy and mobility as intermediate steps. We develop such a method based on a low-temperature description of the interface in terms of kinks. This simple microscopic picture and the results obtained for the velocity of a shrinking grain in 2D provide the basis for the subsequent incorporation of impurities and the derivation of an expression for the interface velocity in 3D.

When the temperature is low, $\beta J \gg 1$, the only allowed spin flips are those that do not increase the total energy. Therefore kink-antikink pairs cannot nucleate at the interface. Barma [15] observed that the interface between the Ising domains can then be represented by a staircase of kinks shown in Fig. 1. The kinetics of kinks reduces to an exclusion process (asymmetric in the presence of magnetic field) [17,18]. Even though steady-state properties of this process (corresponding to a flat field-driven interface of a fixed inclination) are well known, little progress has been made analytically to describe the evolution of a nonuniform kink distribution corresponding to a curved interface.

Let us define the ensemble average density of kinks $\rho(x, t)$ and derive its evolution equation, which is equivalent to Eq. (4). We outline the derivation here and relegate the details to Appendix A. We focus here on the curvature-driven motion while Appendix A includes the effect of the magnetic field. Unimpeded by its neighbors, each kink executes a random walk corresponding to purely diffusive motion. Many kinks can “pile up” at the same site but cannot pass through each other. Via a transformation which inserts an extra lattice site between every pair of neighboring kinks (illustrated in Fig. 2), we map the dynamics of kinks onto the problem of 1D random walkers which cannot occupy the same lattice site. The density of walkers for this symmetric exclusion process obeys a simple diffusion equation [15]. This is true because when two walkers collide, their indices can be exchanged (i.e., their “identities” switched) without affecting their den-

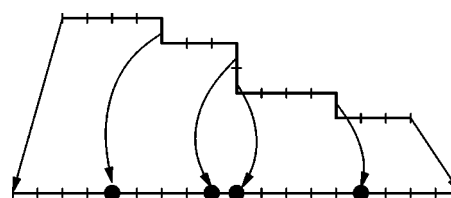


FIG. 2. Mapping of the kink dynamics onto the symmetric exclusion process corresponding to nonoverlapping random walks on a 1D lattice. Note that kinks that pile up vertically in the physical 2D lattice do not overlap in the transformed 1D lattice. See Appendix A for details.

sity. Thus a collision can be viewed as the tunneling of the kinks through each other without affecting each other. The density of hard-core random walkers is insensitive to this identity-switching transformation and must therefore satisfy a diffusion equation. When transformed back to the original coordinate system in which kinks can pile up, the equation for $\rho(x, t)$ reads, for the square lattice (see Appendix A for the triangular lattice version),

$$\tau \rho_t = \left(\frac{\rho_x}{(1 + \rho)^2} \right)_x = -F_x = \mu_{xx}, \tag{6}$$

where subscripts denote differentiation, $F = -\rho_x / (1 + \rho)^2$ is the flux of kinks, and $\mu = -1 / (1 + \rho)$ is the kink “chemical potential.” Equation (6) is a nonlinear diffusion equation with the diffusivity $1 / (1 + \rho)^2$ which is a decreasing function of density. This reduction results from the fact that when more than two kinks occupy the same site, some of these kinks are completely immobile. Since the density of kinks is defined for interfaces inclined with respect to the $\langle 10 \rangle$ orientation, Eq. (6) has to be supplemented by boundary conditions which piece together different $\pi/2$ sectors of the grain boundary.

Geometrically, the density of kinks is the local slope of the interface with respect to the low energy $\langle 10 \rangle$ orientation. It is therefore easy to show that Eq. (4) with $H=0$ and Eq. (6) are equivalent (see Appendix A). Thus we derived the equation of motion for the interface without assuming the applicability of the continuum description of the interface. Even though, for clarity, we have restricted our discussion above to motion by curvature only, we derive in Appendix A the evolution equation for the kink density for general motion by both curvature and an external field, and show that it is equivalent to Eq. (4).

Neglecting thermal excitation of kink-antikink pairs allowed us to construct an equation for a single density of kinks $\rho(x, t)$. In general local densities of kinks ρ_+ and antikinks ρ_- must be considered. Each density obeys the nonlinear diffusion equation (6) augmented by a source term proportional to $\exp(-2\beta J)$, due to the creation of kink-antikink pairs, and a sink term proportional to the product $\rho_+ \rho_-$ due to the annihilation of kinks by antikinks. The local slope of the interface with respect to the low-energy orientation is given by the sum $\rho_+ + \rho_-$ of the kink and antikink densities. Once the details of this two-density approach are worked out, a formal temperature perturbation expansion becomes possible

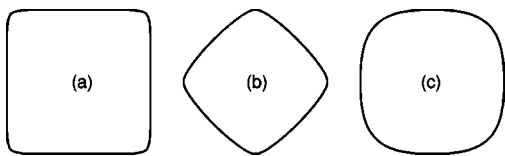


FIG. 3. Shape of an evolving Ising domain in 2D. (a) Final stationary shape of a domain in sufficiently strong negative magnetic field. (b) Shape of a shrinking domain in a large positive field. (c) Self-similar shape of a domain shrinking in absence of magnetic field.

since either ρ_+ or ρ_- is exponentially small in the low-temperature limit. A small mobility for the high-symmetry orientations, which are immobile at zeroth order, will be the most important effect at the next order in the temperature expansion.

C. Evolution of an Ising grain

Let us now use the equation of motion (4) to describe the evolution of an “Ising grain”—i.e., an island of down spins in a sea of up spins. The reduction of the interfacial free energy and spin alignment parallel to a positive magnetic field are the driving forces for the grain shrinkage while negative magnetic field favors grain growth. The numerical method of solving Eq. (4) is described in detail elsewhere [7].

When a sufficiently large negative is applied, the grain grows until it reaches a stationary configuration determined by its initial shape [see Fig. 3(a)]. This happens because the velocity of the interface in the direction of the low-energy planes is never outward since the mobility vanishes for these orientations. Thus a grain cannot grow beyond its initial size. Any growth process has to include the nucleation of kink-antikink pairs which is explicitly ignored in our description.

The amplitude of the positive magnetic field H determines the shape of the shrinking grain. When $\beta H \gg \beta H_c = 1/R$, the second term in Eq. (4) dominates. Note that for large grains this crossover magnetic field vanishes like $1/R$. The shape of the grain shrinking under these conditions, shown in Fig. 3(b), is strongly anisotropic.

When the applied field is much smaller than the crossover field, the evolution is controlled by the more isotropic reduced mobility and thus the shape of a shrinking grain is close to a circle. Even when initially the dynamics is controlled by the magnetic field, the crossover to curvature dominated dynamics will happen when the grain shrinks to a sufficiently small size. In this regime, the grain shrinks in a self-similar manner [see Fig. 3(c)].

Self-similar evolution of the shrinking grain

Here we restrict ourselves to the square lattice while citing the results for the hexagonal lattice in Appendix B. We also set the time scale $\tau=1$.

To compute the shape of a shrinking grain we need to specify the region in which our kink description holds and fix the boundary conditions at the edges of this region. Since we expect the grain to possess four mirror planes inclined at

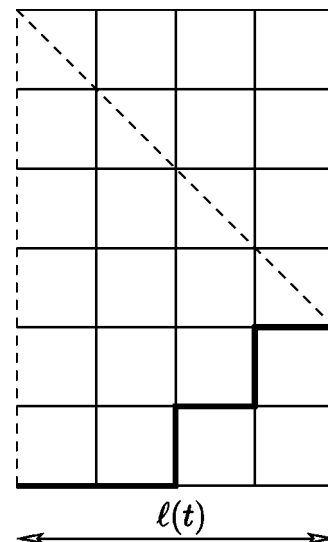


FIG. 4. A $\pi/4$ slice of the grain defined by the dashed lines that converge in the center of the grain. The thick line is the grain boundary. The kink density $\rho(x, t)$ is defined on a shrinking domain of width $\ell(t)$.

0, $\pm\pi/4$ and $\pi/2$ with respect to the $\langle 10 \rangle$ plane, we will restrict ourselves to a $\pi/4$ wedge (see Fig. 4). The slope at the left edge of the wedge ($x=0$) is $\rho=0$ and the slope at the right edge [$x=\ell(t)$] is $\rho=1$ due to mirror symmetry around the $\pi/4$ plane and the smoothness of the grain shape. Thus we are to solve Eq. (6) subject to the boundary conditions

$$\rho(0, t) = 0, \quad \rho(\ell(t), t) = 1. \quad (7)$$

The final ingredient in determining the grain shape is the shrinking rate. The slice width $\ell(t)$ shrinks as the kinks at its right edge flow to the left with a flux $F(\ell) = -\rho_x(\ell)/4$. Every time the kinks move *two* sites to the left, the width of the slice is reduced by 1 (see Fig. 5 for a visual explanation), and therefore

$$\dot{\ell}(t) = \frac{F(\ell)}{2} = -\frac{\rho_x(\ell)}{8}. \quad (8)$$

As we mentioned above, in the absence of a magnetic field, the shape of the shrinking grain is self-similar. To prove this we seek a solution to the moving boundary problem defined by Eqs. (6)–(8), which depends on space and time only through a combination $\zeta = x/\ell(t)$. Substituting this ansatz into the expression for the shrinking rate, Eq. (8), we obtain

$$\ell \dot{\ell} = -\frac{\rho'(1)}{8}, \quad (9)$$

where the prime denotes differentiation with respect to ζ . Thus the rate of change of the grain area $A \sim \ell^2$ under this self-similar evolution is constant as expected. The kink diffusion equation (6) becomes

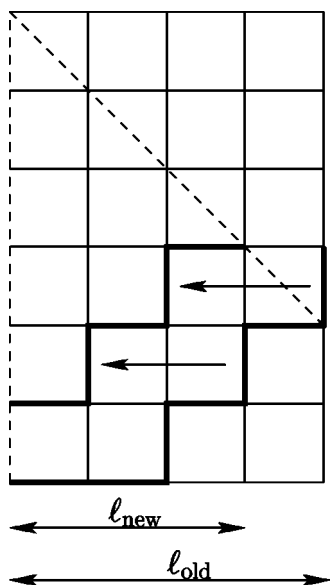


FIG. 5. When the rightmost kink moves two steps to the left, the width of the domain is reduced by 1.

$$B\zeta\rho' = \left(\frac{\rho'}{(1+\rho)^2} \right)', \quad (10)$$

with $\rho(0)=0$, $\rho(1)=1$, and $B=-\ell\dot{\ell}=\rho'(1)/8$. The constant $B \approx 0.331491$ is determined self-consistently by a shooting procedure. Figure 6 shows the comparison of the solution of Eq. (10) to the ensemble-averaged Monte Carlo simulation of diffusing hard-core kinks with boundary conditions appropriate to the shrinking grain scenario. Quantitative agreement of the sharp interface result (4) with the Monte Carlo simulation of the full KIM was found in Ref. [8].

It is useful to recast Eq. (10) in terms of the polar parametrization of the self-similarly shrinking grain $r(\phi, t) = \sqrt{2}\ell(t)r_{2D}(\phi)$. We chose to scale $r(\phi, t)$ in such a way that $r_{2D}(\pi/4)=1$. The kink density of a self-similarly shrinking grain is a function of ϕ only:

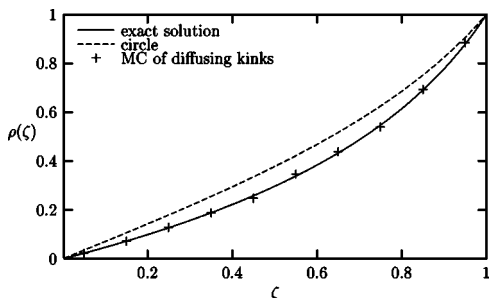


FIG. 6. Density of kinks in units of the inverse lattice constant plotted against the dimensionless scaled distance ζ across the arc. The exact density for a self-similarly shrinking grain obtained by solving Eq. (10) is compared to that obtained via a Monte Carlo simulation of diffusing impermeable kinks. The dashed line shows for comparison the density of kinks in a circular arc on a square lattice.

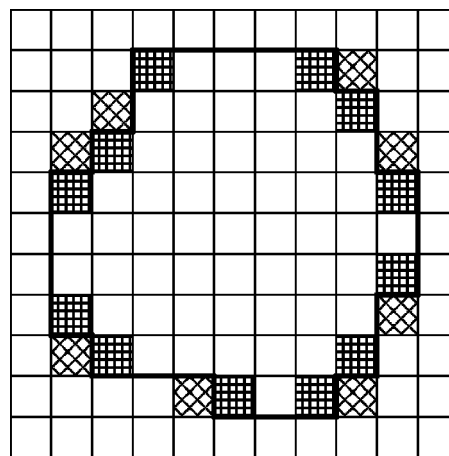


FIG. 7. The number of the outside corner spins (diagonal crosshatch) for any domain is always smaller by 4 than the number of the inside corner spins (horizontal-vertical crosshatch). The shrinking rate of this domain, computed from the difference between the inside and outside corner spins, is thus known exactly in the low-temperature limit.

$$\bar{\rho}(\phi) = \frac{r_{2D}(\phi)\sin\phi - r'_{2D}(\phi)\cos\phi}{r_{2D}(\phi)\cos\phi + r'_{2D}(\phi)\sin\phi}. \quad (11)$$

The equation for the shape of the self-similarly shrinking grain in the polar coordinates can be integrated once to yield

$$2Br_{2D}^2(\phi)[r_{2D}(\phi)(\sin\phi + \cos\phi) + r'_{2D}(\phi)(\sin\phi - \cos\phi)]^2 = r_{2D}^2(\phi) + 2r'_{2D}(\phi) - r''_{2D}(\phi), \quad (12)$$

subject to $r'_{2D}(0)=r'_{2D}(\pi/4)=0$ (by symmetry) and $r_{2D}(\pi/4)=1$. One of these conditions is automatically satisfied for the value of B found above.

Let us finally mention another analytic result concerning the grain shrinking rate dA/dt :

$$-\tau \frac{dA}{dt} = \oint d\phi M_{2D}^*(\phi) = \begin{cases} 4, & \text{square,} \\ 3\sqrt{3}, & \text{hexagonal.} \end{cases} \quad (13)$$

These formulas (the square lattice result first appeared in Ref. [19]) are a simple consequence of the fact that only the corner spins are allowed to flip (see Fig. 7). When a spin in a concave corner flips, the area of the grain increases by 1 (square lattice). And vice versa, when a kink in convex corner flips, the area is reduced by 1. Since the probabilities of all allowed spin flips are the same and the number of convex kinks on a square lattice is greater than the number of concave kinks by 4 (due to Hopf's theorem which states that the rotation index of a simple curve is 1), we arrive at Eq. (13). Reference [8] checked that the shrinking rate on the hexagonal lattice is indeed $3\sqrt{3} \approx 5.196$.

D. Drag by immobile impurities

The kink picture of the low-temperature grain boundary dynamics is useful in understanding the effect of dilute immobile impurities. We model the interaction of the grain boundary with interstitial impurities by defining a variable

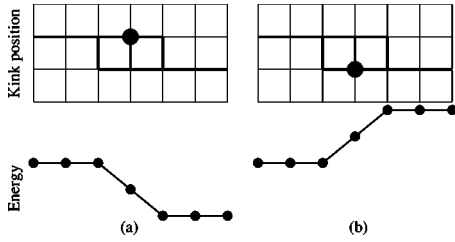


FIG. 8. Illustration of the energy landscape resulting from the interaction of a kink with a single fixed impurity (large solid circle) on the dual lattice. The up (down) spin domain is above (below) the interface represented by a thick black line along the dual lattice. The vertical segments denote three positions of the kink. The energy (in arbitrary units) corresponding to these three positions is shown schematically below. When the impurity is positioned such that the top edge of the kink passes the impurity from left to right, the total energy of the system decreases (a). The opposite is true if the impurity is on the lower edge of the kink (b).

θ_{mn} on the dual lattice sites. $\theta=1$ when an impurity is present and 0 otherwise. The impurities are randomly positioned on the dual lattice and do not move. The interaction of the impurities with the spins is introduced via an additional term in the energy

$$E_{\text{imp}} = \epsilon \sum_{m,n} \theta_{mn} S_{(mn)}, \quad (14)$$

where $S_{(mn)}$ is the total magnetization of the Ising spins nearest to the impurity located at site (m,n) of the dual lattice and the sum is over all the dual lattice sites.

Figure 8 explains graphically that, depending on its position, an isolated impurity provides either a left- or a right-directed short-range force acting on a kink. In addition to this force there is a two-kink effect which makes kink pileups energetically favorable when they occur on the impurity site.

So far we considered only positively charged impurities $\theta=+1$. The interface is attracted to these impurities. Negatively charged impurities with $\theta=-1$ repel the interface. However, the qualitative picture of the kink-impurity interaction presented in Fig. 8 still holds. The only difference is that the effect of the negative impurity on the top edge of the kink is equivalent to the effect of the positive impurity on the bottom edge and vice versa. In the limit of high density of impurities, additional effects due to the interplay of positively and negatively charged impurities become important. For example, a row of alternating positive and negative impurities perpendicular to the interface pulls the interface along in one direction or another due to the ease of nucleating kink-antikink pairs. Additional phenomena arise when both positively and negatively charged impurities are presented. Exploring these phenomena is outside the scope of this article.

The diffusing kink picture is especially simple when the impurities are dilute and $\epsilon \gg J \gg kT$. In this limit the kinks diffuse only downslope in the static energy landscape produced by the impurities. When impurities are dilute, this energy landscape consists of a number of flat terraces bound by steep vertical cliffs or walls. The kinks diffuse and fall down

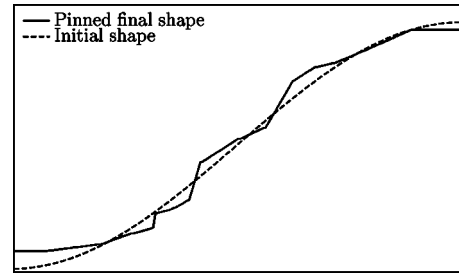


FIG. 9. Time-averaged shape of a grain boundary pinned by strong $\epsilon=5$ impurities which occupy 1% of the dual lattice sites is a collection of straight segments obtained via a Monte Carlo simulation of the 2D Ising model with an additional energy given in Eq. (14).

cliffs until they fall onto a terrace which is bound by walls on both sides. The kinks become trapped on this terrace. In the long-time limit, the density of the trapped kinks becomes uniform on this terrace. This means that the slope of the piece of grain boundary which corresponds to this terrace is a constant given by the density of the trapped kinks. This density depends on the initial distribution of kinks and impurities and can be anything. Therefore, in this limit, the grain boundary is pinned and consists of a series of flat facets of random length and inclination.

Figure 9 presents results of the Monte Carlo simulation of the low-temperature 2D Ising model in the presence of strong dilute positively charged immobile impurities. What is shown is the time-averaged location of the boundary between the spin-up and spin-down domains. The boundary is pinned and consists of straight pieces of random length and orientation. Impurities are located at either end of each such facet. This result supports our qualitative picture.

Addition of magnetic field introduces yet another energy scale H into the picture. When $H \ll \epsilon$, the boundary is pinned. The shape of the pinned facets depends on the relative size of $1/\beta H$ and length of the pinned facet L . In equilibrium, the kink drift due to the magnetic field is balanced by the diffusion due to curvature. Thus small facets for which $L \ll 1/\beta H$, remain straight. Conversely, when $L \gg 1/\beta H$, the long facets look like the corners of a droplet expanding in coaligned magnetic field whose shape is given in Fig. 3(a).

Strong positive impurities ($\epsilon \gg J$) in the bulk of a domain of aligned spins always have two spins near them that are antialigned with the rest of the spins in that domain. Thus impurities serve as nuclei for the formation of droplets of the phase of spins aligned with the applied magnetic field. Conversely, strong negatively charged impurities favor alignment of the nearby spins and thus can inhibit nucleation of the phase favored by the application of magnetic field.

III. THREE-DIMENSIONAL ISING MODEL

Whereas a curve on a plane can be characterized by a single scalar curvature, a smooth surface embedded in a three-dimensional space is characterized by a rank-2 tensor $L_{\alpha\beta}$ ($\{\alpha, \beta\}=1, 2$). This tensor is called the second fundamental form or the Weingarten map or just the curvature

tensor. Half the trace of this tensor is the mean curvature, while its determinant is the Gaussian curvature. This tensor is defined at some point P by selecting an orthogonal coordinate system x_α in the tangent plane at P and writing

$$L_{\alpha\beta} = \hat{t}_\alpha \cdot \frac{\partial \hat{n}}{\partial x_\beta}, \quad (15)$$

where \hat{t}_α are the unit tangent vectors and \hat{n} is the unit normal to the surface.

The reduced mobility of a two-dimensional interface is also a rank two tensor $M_{\alpha\beta}^*$ which when contracted with the curvature tensor yields the normal velocity of the interface:

$$v = \sum_{\alpha,\beta} M_{\alpha\beta}^* L_{\beta\alpha}. \quad (16)$$

The reduced mobility tensor depends on the scalar bare mobility M_{3D} (found, for example, by measuring the speed of a driven flat interface) and the interfacial free energy γ and its derivatives. In the neighborhood of the point P the normal \hat{n} is specified by the deviations φ_1 and φ_2 from the normal at P in the directions \hat{t}_1 and \hat{t}_2 . The free energy is a function of the normal \hat{n} and therefore, in the neighborhood of P , a function of these angles $\gamma_{3D}(\varphi_1, \varphi_2)$. The reduced mobility tensor is then defined as

$$M_{\alpha\beta}^* = M_{3D} \left(\gamma \delta_{\alpha\beta} + \frac{\partial^2 \gamma}{\partial \varphi_\alpha \partial \varphi_\beta} \right). \quad (17)$$

Since our Kinetic Monte Carlo (KMC) simulations show that the shape of a 3D shrinking grain is even closer to a sphere than a 2D shape to a circle, this reduced mobility tensor is nearly isotropic. This isotropy allows us to predict the 3D grain shrinking rate [defined as the rate of change of the 2/3 power of its volume $S \equiv (d/dt)V^{2/3}$] by calculating the velocity v_{100} of the shrinking grain boundary at the $\langle 100 \rangle$ orientation. We will first estimate this velocity within the terrace-step-kink description of the vicinal surface. We then derive an exact expression for this velocity within the continuum limit.

A. Shrinking terrace view of the dynamics near $\langle 100 \rangle$ plane

The low-temperature interface can be described within the terrace-step-kink (TSK) model [20]. When steps are far apart, each step obeys the dynamics of a 2D grain. If the 3D grain is a sphere of radius R , it is described near the $\langle 100 \rangle$ orientation by a stack of circular terraces of increasing radii $r_1(t)$, $r_2(t)$, etc. (see Fig. 10). Because these steps are part of the spherical grain, they are related via

$$\sqrt{R^2 - r_2^2} + 1 = \sqrt{R^2 - r_1^2}. \quad (18)$$

Solving this equation for R^2 , differentiating with respect to time and using the exact expression for the 2D grain shrinking rate (13) $r_1 \dot{r}_1 = r_2 \dot{r}_2 = -2/\pi$ we obtain $R \dot{R} = -2/\pi$. Therefore, within the spherical grain approximation, the grain shrinking rate is

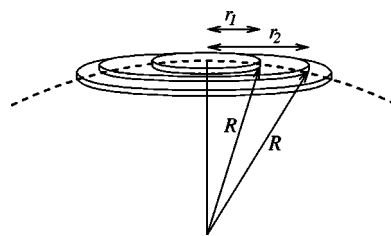


FIG. 10. Grain shape near the 100 plane can be viewed as a collection of terraces.

$$S \approx - \left(\frac{4\pi}{3} \right)^{2/3} \frac{4}{\pi} \approx -3.309, \quad (19)$$

which is in reasonable good quantitative agreement with the shrinking rate found by KMC simulations $S = -3.335 \pm 0.001$.

B. Low-temperature expansion of interface free energy and mobility near the $\langle 100 \rangle$ plane

Little analytical progress in deriving equilibrium and kinetic properties of the 3D KIM has been achieved to date. A mean-field expression for the free energy of the TSK model neglecting step-step interaction was obtained by Gruber and Mullins [21]. Holzer and Wortis [22] calculate the free energy near the $\langle 100 \rangle$ plane in the more controlled diagrammatic temperature expansion. It is sufficient for our purposes to keep only the leading term in the expansion

$$\gamma_{3D}(\theta, \phi) \approx \theta \gamma_{2D}(\phi), \quad (20)$$

where θ is the angle between the normal to the interface \hat{n} and the z axis (which is the normal to the $\langle 100 \rangle$ plane) and ϕ is the angle between the projection of \hat{n} onto the x - y plane and the x axis counted clockwise. Formula (20) is simply a statement that the free energy of a vicinal surface is composed of the free energies of the steps (considered to be noninteracting).

In the same noninteracting step approximation, the bare mobility of the vicinal surface is

$$M_{3D}(\theta, \phi) \approx \theta M_{2D}(\phi). \quad (21)$$

C. Speed of the $\langle 100 \rangle$ orientation of the shrinking grain

The expressions for the interfacial free energy and the mobility in the vicinity of the $\langle 100 \rangle$ plane allow us to calculate the reduced mobility at this orientation as well as the grain shape in the neighborhood of the point P where the normal is in the z direction.

Let the shape of the grain in cylindrical coordinates be $z(r, \phi) = r^2 / r_{2D}^2(\phi)$. The shape of the $z=1$ section of the 3D grain is $r = r_{2D}(\phi)$ in polar coordinates. A circular terrace—i.e., $r_{2D}(\phi) = \sqrt{2}R$ —corresponds to a sphere of radius R . We choose this suggestive parameterization of the 3D shape with the foresight that $r_{2D}(\phi)$ will turn out to be identical to the shape of the self-similarly shrinking 2D grain. This is not surprising in view of the shrinking terrace picture of the 3D

grain evolution near the $\langle 100 \rangle$ orientation of the previous subsection.

Given the shape of the 3D grain, we can compute the normal of the surface $\hat{n}(r, \phi)$ and the curvature tensor $L_{\alpha\beta}(r, \phi)$. The reduced mobility tensor $M_{\alpha\beta}^*(\hat{n})$, in turn, can be calculated using the free energy expression (20) following

$$\lim_{r \rightarrow 0} v(r, \phi) = - \frac{2[r_{2D}^2(\phi) + 2r'_{2D}(\phi) - r''_{2D}(\phi)]}{r_{2D}^2(\phi)[r_{2D}(\phi)(\sin \phi + \cos \phi) + r'_{2D}(\phi)(\sin \phi - \cos \phi)]^2} = \text{const}, \quad (22)$$

subject to the smoothness constraints $r'_{2D}(0) = r'_{2D}(\phi) = 0$. The function $r_{2D}(\phi)$ which satisfies the above equation and constraints is precisely the self-similar shape of a 2D shrinking grain. If we set the size of the 3D grain by choosing $r_{2D}(\pi/4) = \sqrt{2}R$, we arrive at $v = -2B/R$ and hence (again assuming a spherical shape to estimate the volume)

$$S \approx - \left(\frac{4\pi}{3} \right)^{2/3} 4B \approx -3.445. \quad (23)$$

Since the diameter of the self-similar shape at $\phi=0$ is slightly smaller than its diameter at $\phi=\pi/4$, a better approximation would have been to scale r_{2D} in such a way that at the intermediate angle $r_{2D}(\pi/8) = \sqrt{2}R$.

IV. CONCLUSIONS

In summary, using a kink-based description, we have derived directly from a microscopic model (low-temperature KIM) a continuum evolution equation for the anisotropic motion of a simple interface, and we have shown its equivalence to the standard phenomenological law of motion by curvature. We have illustrated with the example of dilute impurities that this kink-based kinetic description provides a useful framework for studying more complex situations. By extending this description to 3D and by exploiting our 2D result for the self-similar dynamics of shrinking terraces, we have obtained the velocity of a curved interface near a singular orientation. We have shown that even though the interface stiffness tensor and the curvature tensor are singular at the $\langle 100 \rangle$ orientation, their product, which determines the interface velocity, is smooth. Furthermore, this velocity is consistent with the one predicted from the 3D tensorial generalization of the law for anisotropic curvature-driven motion using known expressions for the interface free energy and bare mobility.

Our kink-based derivation of a continuum equation of interface motion highlights the microscopic mechanism for the remarkable isotropy of the reduced mobility in both 2D and 3D and thus the shape of grains shrinking under the influence of capillarity alone. The reduced mobility is a product of the interfacial stiffness and the interfacial mobility both of which are strongly anisotropic. The isotropy of the reduced mobil-

ity is therefore a result of the cancellation of anisotropies of the interfacial stiffness and interfacial mobility. The microscopic reason for the cancellation is purely geometric in origin. The number of geometrically necessary kinks—and hence the configurational entropy of the interface—varies rapidly with inclination near low-energy and low-mobility orientations, but slowly near high-energy and high-mobility interfaces, where the density of kinks is high. Since the leading-order contribution to the interfacial stiffness comes from configurational entropy, stiffness is high where mobility is low and vice versa. The cancellation of anisotropies leads to roughly isotropic reduced mobility. Therefore the shape of a shrinking grain can appear isotropic or anisotropic depending on whether driving forces other than capillarity are present. The bare mobility of the interface is, however, independent of the nature of the driving force.

An interesting prospect for the future is to extend this kink-based theoretical description of interface motion to realistic, and more complex, grain boundaries where kinks have the character of dislocations. Work along this line is presently in progress.

ACKNOWLEDGMENTS

We thank Bernard Derrida, Mikhail Mendelev, Anthony Rollet, and David Srolovitz for valuable discussions. This research is supported by U.S. DOE through Grant No. DE-FG02-92ER45471 and funds from the Computational Materials Science Network.

APPENDIX A: DERIVATION OF THE KINK EQUATION OF MOTION

In general, kinks comprising the grain boundary are characterized by their width b , which is the distance of the closest approach of two neighboring kinks, their height d , and the length of the steps of their random walk a . For example, on a square lattice, $d=a$, the lattice constant and $b=0$, while on a triangular lattice $d=a\sqrt{3}/2$ and $b=a/2$. In the continuum limit, we define the density of kinks $\rho(x, t)$ and seek its evolution equation in some fixed domain $x \in [x_L, x_R]$. Since neighboring domains contain antikinks, absorbing boundary conditions must be imposed $\rho(x_L, t) = \rho(x_R, t) = 0$.

A special case of this problem $a=b$ describes random walkers in 1D which cannot occupy the same site. When a magnetic field is present, the random walk is biased and the problem can be mapped onto the well-studied asymmetric exclusion process [17,23]. To map the problem of finding the evolution of the kink density $\rho(x,t)$ onto this special problem, we insert a space $c=a-b$ between each pair of adjacent kinks, as illustrated for a square lattice in Fig. 2. The resulting kink density $R(\xi,t) \in [0,1/a]$ is defined in a different domain $\xi \in [\xi_L(t), \xi_R(t)]$. In the presence of magnetic field H , this kink density satisfies the equation [17,24] (subscripts denote differentiation)

$$R_t = DR_{\xi\xi} + \alpha[R(1-aR)]_{\xi} = -J_{\xi}, \quad (A1)$$

$$J(\xi,t) = -DR_{\xi} - \alpha R(1-aR),$$

where $D=a^2/2\tau$, $\alpha=a\beta H/\tau$, τ is the Monte Carlo time step, and J is the flux of kinks in the moving ξ domain. Note that this equation is identical to Burger's equation after elimination of the drift term αR_{ξ} by transformation to a moving frame. As kinks annihilate at the boundaries of the x domain, the ξ domain shrinks. Each kink that leaves the x domain, decreases the ξ domain by c . This implies that the boundaries of the ξ domain move with a velocities proportional to the current of kinks out of the domain:

$$\dot{\xi}_L = -cJ(\xi_L(t),t), \quad \dot{\xi}_R = -cJ(\xi_R(t),t). \quad (A2)$$

The equations for the motion of boundaries, Eqs. (A2), together with the absorbing boundary conditions

$$R(\xi_L(t),t) = R(\xi_R(t),t) = 0, \quad (A3)$$

completely define the problem of diffusing kinks in the ξ domain.

The mapping is inverted via

$$\xi(x,t) - \xi_L(t) = x - x_L + c \int_{x_L}^x \rho(x',t) dx'. \quad (A4)$$

At some fixed time we can write

$$R(\xi,t) d\xi = \rho(x,t) dx, \quad (A5)$$

since both expressions give the number of kinks in the same physical interval. Using Eq. (A4) we obtain

$$R(\xi,t) = \frac{\rho(x,t)}{1+c\rho(x,t)} \quad \text{or} \quad \rho(x,t) = \frac{R(\xi,t)}{1-cR(\xi,t)}. \quad (A6)$$

This relationship (A5) allows us to invert Eq. (A4) to obtain

$$x(\xi,t) - x_L = \xi - \xi_L(t) - c \int_{\xi_L(t)}^{\xi} R(\xi',t) d\xi'. \quad (A7)$$

It is now only a matter of carrying out the chain rule together with the boundary conditions (A3) and the transformation (A4) to obtain

$$R_{\xi} = \frac{\rho_x}{(1+c\rho)^3}, \quad (A8a)$$

$$R_t = \frac{\rho_t}{(1+c\rho)^2} - D \frac{c\rho_x^2}{(1+c\rho)^5} - \alpha \frac{\rho_x c\rho(1-b\rho)}{(1+c\rho)^4}, \quad (A8b)$$

$$R_{\xi\xi} = \frac{\rho_{xx}}{(1+c\rho)^4} - \frac{3c\rho_x^2}{(1+c\rho)^5}. \quad (A8c)$$

Thus we obtain the nonlinear diffusion equation for $\rho(x,t)$ which reads

$$\rho_t = D \frac{\rho_{xx}}{(1+c\rho)^2} - 2cD \frac{\rho_x^2}{(1+c\rho)^3} + \alpha \frac{\rho_x(1-2b\rho-bc\rho^2)}{(1+c\rho)^2} = -F_x, \quad (A9)$$

where

$$F = -D \frac{\rho_x}{(1+c\rho)^2} - \alpha \rho \frac{1-b\rho}{1+c\rho} \quad (A10)$$

is the flux of kinks in the fixed domain which vanishes at zero kink density.

Using the relationship of the local slope and kink density $\tan \phi = h_x(x,t) = d\rho(x,t)$ and the expressions for the normal interface velocity and curvature,

$$v_n = \frac{h_t}{(1+h_x^2)^{1/2}}, \quad \kappa = \frac{h_{xx}}{(1+h_x^2)^{3/2}}, \quad (A11)$$

we can compute the bare and reduced mobilities from the normal velocity of the interface $v_n = M^* \kappa + MH$. We obtain

$$M^* = \frac{D}{(\cos \phi + \nu \sin \phi)^2}, \quad M = \frac{\beta \lambda \sin \phi (\cos \phi - \mu \sin \phi)}{\tau \cos \phi + \nu \sin \phi}, \quad (A12)$$

where $\nu=c/d$, $\mu=b/d$ and $\lambda=a/d$ are geometric factors. These expressions are valid for $\phi \in [0, \pi/4]$ for the square lattice and for $\phi \in [0, \pi/6]$ for the triangular lattice.

APPENDIX B: SELF-SIMILAR SHRINKING GRAIN ON A HEXAGONAL LATTICE

The symmetry of the hexagonal lattice allows us to solve for the shape of the self-similarly shrinking grain in a $\pi/6$ wedge. We present yet another way of obtaining this shape. Let the points on the boundary be labeled by ϕ , the azimuthal angle $\phi \in [0, \pi/6]$. Let $\theta(\phi)$ be the local slope and $r_{2D}(\phi)$ the radial distance from the center of the grain. The shrinking shape will remain self-similar if the radial velocity v_r at each point of the boundary is proportional to the radius at that point. The normal velocity $v_n = M^* \kappa$ is the projection of the radial boundary velocity onto the normal direction. The curvature is the derivative of the slope with respect to the arc length:

$$\kappa = \frac{d\theta}{ds} = \frac{\theta' \cos(\phi - \theta)}{r_{2D}}. \quad (B1)$$

Thus, the condition of the self-similarity of the shrinking

shape can be written as

$$v_r = \frac{v_n}{\cos(\phi - \theta)} = M^* \frac{\theta'}{r_{2D}} = Cr_{2D}, \quad (\text{B2})$$

where C is some proportionality constant. To complete the description we need to express the radius $r_{2D}(\phi)$ in terms of $\theta(\phi)$:

$$r'_{2D}(\phi) = r_{2D}(\phi) \sin[\phi - \theta(\phi)]. \quad (\text{B3})$$

Without loss of generality we set $r_{2D}(0)=1$ and integrate Eqs. (B2) and (B3) together up to $\phi=\pi/6$. The second boundary θ -boundary condition $\theta(\pi/6)=\pi/6$ selects a unique C . The numerical shooting yields $C \approx 0.903\,535$. The shape of the self-similarly shrinking grain on a hexagonal lattice is remarkably close to a circle. The largest and smallest grain diameters differ by only 0.4%.

-
- [1] M. Winning, G. Gottstein, and L. S. Shvindlerman, *Acta Mater.* **50**, 353 (2002).
- [2] D. A. Molodov, G. Gottstein, F. Heringhaus, and L. S. Shvindlerman, *Mater. Sci. Forum* **294**, 127 (1999).
- [3] C. Herring, in *The Physics of Powder Metallurgy*, edited by W. E. Kingston (McGraw-Hill, New York, 1949).
- [4] M. Hillert, *Scr. Metall.* **17**, 237 (1983).
- [5] Y. Huang and F. J. Humphreys, in *Proceedings of the 1st International Conference on Recrystallization and Grain Growth*, edited by G. Gottstein and D. A. Molodov (Springer, Aachen, Germany, 2001), pp. 409–414.
- [6] D. A. Molodov, G. Gottstein, F. Heringhaus, and L. S. Shvindlerman, *Acta Mater.* **46**, 5627 (1998).
- [7] M. I. Mendeleev, D. J. Srolovitz, G. Gottstein, and L. S. Shvindlerman, *J. Mater. Res.* **17**, 234 (2002).
- [8] A. E. Lobkovsky, A. Karma, M. I. Mendeleev, M. Haataja, and D. J. Srolovitz, *Acta Mater.* **52**, 285 (2004).
- [9] R. J. Glauber, *J. Math. Phys.* **4**, 294 (1963).
- [10] C. Rottman and M. Wortis, *Phys. Rev. B* **24**, 6274 (1981).
- [11] J. E. Avron, H. Van Beijeren, L. S. Schulman, and R. K. P. Zia, *J. Phys. A* **15**, L81 (1982).
- [12] M. S. Kochanski, *J. Phys. A* **32**, 1251 (1999).
- [13] M. A. Yurishchev, *Phys. Rev. E* **55**, 3915 (1997).
- [14] H. Spohn, *J. Stat. Phys.* **71**, 1081 (1993).
- [15] M. Barma, *J. Phys. A* **25**, L693 (1992).
- [16] P. A. Rikvold and M. Kolesik, *J. Stat. Phys.* **100**, 377 (2000).
- [17] T. M. Liggett, *Interacting Particle Systems* (Springer-Verlag, New York, 1985).
- [18] A. D. Masi, N. Ianiro, A. Pellegrinotti, and E. Presutti, in *Nonequilibrium Phenomena II: from Stochastics to Hydrodynamics*, edited by J. L. Lebowitz and E. W. Montroll (Elsevier, New York, 1984).
- [19] D. Kandel and E. Domany, *J. Stat. Phys.* **58**, 685 (1990).
- [20] W. K. Burton, N. Cabrera, and F. C. Frank, *Philos. Trans. R. Soc. London, Ser. A* **243**, 299 (1951).
- [21] E. E. Gruber and W. W. Mullins, *J. Phys. Chem. Solids* **28**, 875 (1967).
- [22] M. Holzer and M. Wortis, *Phys. Rev. B* **40**, 11 044 (1989).
- [23] B. Derrida, E. Domany, and D. Mukamel, *J. Stat. Phys.* **69**, 667 (1992).
- [24] H. Spohn, *Large Scale Dynamics of Interacting Particles* (Springer-Verlag, New York, 1991).